# A Novel Approach to Acoustic Liquid Density Measurements Using a Buffer Rod Based Measuring Cell

Erlend Bjørndal, *Member, IEEE*, Kjell-Eivind Frøysa, and Svein-Atle Engeseth

*Abstract*—A new method for measuring the pressure reflection coefficient in a buffer rod configuration is presented, together with experimental results for acoustic measurements of the liquid density, based on the measurement of the liquid's acoustic impedance. The method consists of using 2 buffers enclosing the liquid in a symmetrical arrangement with a transducer fixed to each buffer. One of the transducers is used in a pulse-echo mode while the other transducer operates as a receiver. The echo amplitudes leading to the pressure reflection coefficient as found by this method possess advantages such as reduced attenuation due to a shorter liquid transmission path and reduced interference, as compared with the ABC method. Measurements with distilled water and with special density calibration oil qualities have been performed using both the new method and the ABC method and are shown for the new method to give a density span within ±0.15% of the reference values. A comparison of the measured densities based on both a time-domain and a $l^2$-norm frequency domain integration signal processing approach is given, along with a recommendation as to how the signal processing should be performed.

## I. INTRODUCTION

D ENSITY is a material property of utmost importance in many fields, such as the process industry in general, and also for fiscal use. Applications are in such diverse fields as flow measurement, fluid characterization, biomedical diagnostics, process control in industry, and quality control in the food and beverage industry. The liquid density measurements by acoustic methods are mainly performed by use of the acoustic impedance $Z$ and the compressional wave sound speed $c$ by use of the relation $Z = \rho c$. The acoustic impedance is normally found by use of the pressure reflection and transmission coefficients at the interface between a reference material and a liquid sample.

A simple and well-known method for obtaining the pressure reflection coefficient $R$ (named just reflection coefficient for simplicity) is to use a transducer in pulse-echo

mode with the transducer element fixed to a buffer. Then, during the calibration phase, 2 measurements are needed. One is performed in air and a second measurement is performed with liquid inserted between the buffer and a reflector [1]–[3]. This method requires frequent calibration due to thermal drift and aging of the electronics and sensor components. A reference acoustic path would reduce such problems, because part of the transmitted signal would be available for automatic calibration purposes.

Papadakis [4] developed the ABC method for measuring the acoustic impedance and the attenuation in solids based on a triple-echo buffer rod approach where the reflection coefficient is obtained from the measured amplitude ratios. However, this approach may be prone to severe attenuation of the third echo signal because it has traversed the sample 4 times along with the possibility of interference effects of the echo signals from the ring-down in the buffer or from mode converted echo signals from the buffer-sample interface.

Other reference path approaches applied for acoustic liquid density measurements also exist. Püttmer *et al.* [5] used a buffer on the backside of the transducer element, allowing the transducer element to sense the transmitted signal amplitude, as reflected from the backside buffer-air interface. Adamowski *et al.* [6]–[8] actually used the ABC method by including a large diameter membrane receiver between 2 buffer rods in front of the transmitter element for the elimination of the sound field diffraction effect. Hirnschrodt *et al.* [9], [10] used a solid layer separating a reference liquid and a test liquid for increased sensitivity, due to the behavior of the solid layer as "invisible" at given frequencies of the incident sound field, making the solid layer appear a half-wavelength thick. Delsing *et al.* [11]–[13] used 2 buffers of different materials between the transducer element and the liquid.

In addition to being able to give the acoustic impedance of the sample, along with the buffer and the liquid sound speeds, the sample density and, thereby, the adiabatic compressibility, the ABC method of Papadakis [4] can be used for fluid characterization, because it can also give the sample attenuation. Therefore, it was decided to try to further develop this method, and at the same time obtain reduced influence from the aforementioned weaknesses concerning this method. This led to the development of 2 new generic approaches for the measurement of the reflection coefficient, from which some of the proposed methods were shown to possess lower uncertainty than the ABC
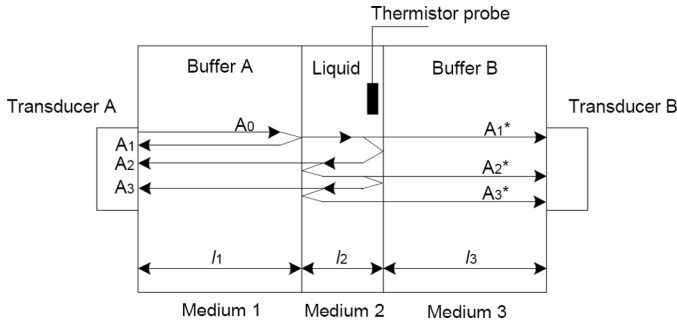
Fig. 1. Schematic view of the proposed measurement principle containing 2 transducers in addition to 2 buffers enclosing the sample liquid. Only the operational mode of using Transducer A in pulse-echo mode is indicated.

method. This was based on analysis of uncertainty contributions from bit resolution and noise only [14].

The further development was performed by using 2 buffers enclosing the liquid in a symmetrical arrangement, with a transducer fixed to each of the buffers, according to Fig. 1.

Section II presents the measurement principle. The instrumentation setup is given in Section III, along with a description of the acquisition system and the calibration approach used. Section IV discusses the signal processing approach and the use of diffraction correction, and Section V presents the measurement cell's mechanical and dimensional design. Section VI presents the measurement results for distilled water and for various calibration oils, which have densities accurately characterized versus temperature. A limited uncertainty analysis is given in Section VII. In Section VIII, the discussion is given, and conclusions are given in Section IX.

## II. Measurement Principle

The description of the measuring principle can be given with respect to Fig. 1, which is seen to consist of one transducer operating in pulse-echo mode (transducer A), together with a receive transducer operating in a through-transmission mode in the other end of the measuring cell (transducer B). The operation can also be reversed, using transducer B in pulse-echo mode, with transducer A as a receiver. The buffers are assumed to be identical, i.e., to have the same dimensions and be made of the same material. In the following, transducer A will be assumed to operate in pulse-echo mode (Tx-transducer), while transducer B will be assumed to operate as a receiver (Rx-transducer).

Here, a maximum number of 3 echo signals on each transducer will be assumed throughout for the analysis.

Measurements by only 2 of the relative amplitude approach methods as given in [14] will here be presented. These are the ABC method of Papadakis [4] using only one transducer, and the newly proposed $R\_echo12\_12$ method using the first 2 echo signals from both transducers. See [14], (44), with $b = -2$ and $d = 0$ for the ABC method,
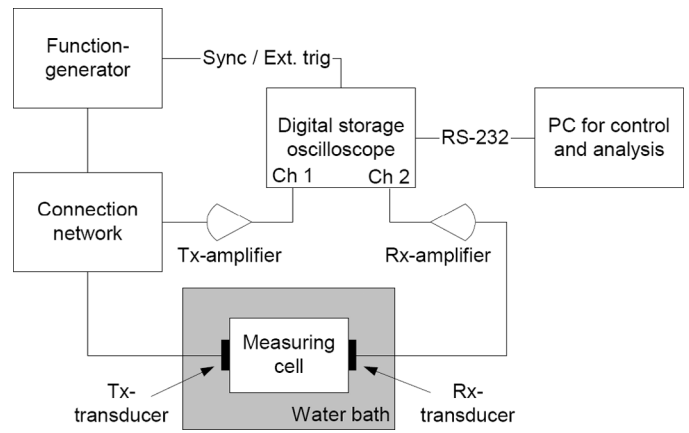


Fig. 2. Block diagram of the measuring system.

and $b = -1$ and $d = -1$ for the $R\_echo12\_12$ method. The reflection coefficients are

$$R = \pm \left(1 - \frac{A_2^2}{A_1 A_3}\right)^{-0.5} \tag{1}$$

$$R = \pm \left(1 - \frac{A_2 A_1^*}{A_1 A_2^*}\right)^{-0.5}, \tag{2}$$

for the ABC and for the $R\_echo12\_12$ method, respectively.

Using a buffer rod configuration measurement cell, the reflection coefficient can be obtained from the acoustic impedance of the buffer and of the liquid, using the plane-wave expression for the reflection coefficient according to

$$R = \frac{Z_2 - Z_1}{Z_1 + Z_2} = \frac{\rho_2 c_2 - \rho_1 c_1}{\rho_1 c_1 + \rho_2 c_2}, \tag{3}$$

from which the liquid density can be expressed as

$$\rho_2 = \frac{\rho_1 c_1 (1 + R)}{c_2 (1 - R)}. \tag{4}$$

The liquid density is therefore seen to depend on the sound speed and the density of the buffer in a proportional manner, whereas it is inversely proportional to the sound speed of the liquid. The liquid density is seen to depend on the reflection coefficient in a nonlinear manner.

## III. Instrumentation

### A. Introduction

A block diagram of the measuring system is given in Fig. 2. The main components are a function generator (Agilent 33220A, Agilent Technologies, Santa Clara, CA), 2 broadband ultrasound transducers (Panametrics 1″ diameter immersion type Videoscan V307-SU 5.0 MHz center frequency, Olympus NDT, Waltham, MA), a measurement cell (described later), a high-speed digitizing oscilloscope (Agilent 54642A, 500 MHz bandwidth, Agilent Technologies), 2 custom-made low noise preamplifiers for signal accommodation, and a PC for control and analysis
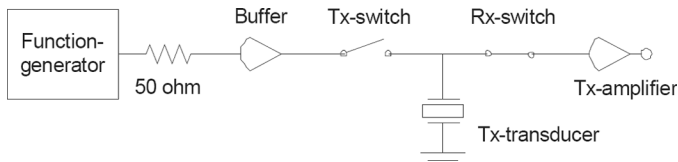
Fig. 3. Switching arrangement for the Tx-transducer.

of the measurements. The measuring cell was placed in a thermostat-regulated water bath keeping the temperature at a given level.

### B. Operational Cycle

The operational cycle can be described in the following way: The generator feeds the transmit transducer with a sinusoidal burst of a predetermined number of periods through a connection network. This process continues for a predetermined number of times, where the acquisition is performed in a coherent fashion by the oscilloscope. The custom-made low-noise preamplifiers were used to accommodate the signal levels to suitable levels for the acquisition by the oscilloscope, and the measured data were presented to the PC over the RS232 serial interface. The preamplifiers have a gain of approximately 50 dB and a gain-bandwidth product of 1 GHz.

### C. Electronic System

The simplest possible form of the connection network consists of a direct connection between the function generator, the Tx-transducer, and the Tx-amplifier, where the 50 Ω output resistance of the function generator serves to avoid complete damping of the received echo signals from the Tx-transducer. However, the noise level experienced for such a direct connection, particularly at the Tx-transducer, was seen to be quite high. This noise level was found not to be influenced by the excitation level directly, but to the range of the excitation level as correlated to some internal relay setting in the function generator. To improve the signal-to-noise-ratio (SNR), a switch arrangement was designed according to Fig. 3.

The switching network consists of an arrangement of 2 switches connected in series with opposite action, with the Tx-transducer connection in-between. The operational mode of the switches is as follows: The Tx-switch is initially active, making a connection between the signal source and the Tx-transducer. After the source has fed the Tx-transducer with the predetermined number of periods, the Tx-switch is opened and the Rx-switch is closed to let the echo signals be acquired. Then the Rx-switch opens and the Tx-switch closes for the next operational cycle. The switches are of the break-before-make type.

The switching network was implemented based on a Supertex HV20720 high-voltage switch with a relatively high on-resistance of 22 Ω, and with a 5 μs turn-on and turn-off time.

In addition, a buffer amplifier with high current drive capacity (LT1210, Linear Technology, Milpitas, CA) was used to obtain a low output impedance. Also, at the receiver end, a low-noise preamplifier (LT1226, Linear Technology) accommodated the signal levels, and an LT1210 buffer was used to drive some short length 50 Ω coaxial cables connecting to the oscilloscope inputs, which were used in 1 MΩ input impedance mode. Due to the given offset range for the oscilloscope, the maximum echo signal had to exceed a peak-to-peak voltage of 1.6 V on the Tx oscilloscope channel.

### D. Temperature Measurement System

The temperature measuring system was based on a Hart Scientific 5665 Thermistor Probe and a Hart Scientific 5611 Thermistor Probe (Hart Scientific, American Fork, UT), both of which have an uncertainty of 0.01°C. The choice of which probe to use was dictated by the path length of the liquid layer. The given probe was inserted into the sample liquid without interfering with the sound field. The temperature reading device was a $6\frac{1}{2}$ digit digital multimeter (Agilent 34401A, Agilent Technologies) operating in a 4-wire configuration, adding a negligible uncertainty to the temperature measurement compared with the given probe uncertainty.

### E. Acquisition Phase

The pulse-repetition rate was set at approximately 100 Hz for the received echoes to die completely out before excitation of the next burst cycle. The echo sequence was averaged a given number of times by the oscilloscope being externally triggered by the function generator, using a sampling rate of 500 MSa/s. The oscilloscope can give out 2000 measuring points in average mode, using a built-in decimation and interpolation procedure, resulting in a raw data time resolution in the range of 15 to 17 ns for the measuring cells used. The oscilloscope was used in a bandwidth limit mode having a 25 MHz cutoff low-pass characteristic. The effect of the oscilloscope built-in low-pass filter was to reduce the bandwidth from the 250 MHz Nyquist rate, giving a 3 dB increase in the SNR for each divide-by-2 factor of cutoff frequency [15]. This gave an increase in SNR of approximately 13 dB beyond the wideband characteristic. The oscilloscope has a basic voltage resolution of 8 bits. Using the average mode, and using measurements on repetitive signals, however, the voltage resolution can be increased to 12 bits maximum, depending on the number of averages used. For each 4-fold increase in the number of averages, one bit of voltage resolution is gained [16], implying an average of 256 for obtaining 12 bits of resolution. The average temperature along with the min/max values during the collection of the acoustic echo signals involved were also acquired.

### F. Calibration

As seen from (4), the following parameters must be known to measure the liquid density: the buffer acoustic

| Temperature [°C] | Density of buffer [kg/m$^3$] |
|---|---|
| 19.874 | 2712.6840 |
| 39.991 | 2708.8823 |

impedance (density and sound speed), liquid sound speed, and the reflection coefficient. The calibration approach used involves obtaining the liquid path length from the distilled water's sound speed dependence on temperature, as given by a 5th order polynomial presented by Marczak [17]. The buffer density was measured by a weighing procedure at Teknologisk Institutt, Ågotnes, Norway, at 2 different temperatures as given in Table I, with an absolute uncertainty of less than 36 ppm. A linear fit was used between those temperatures. Then, the acoustic impedance of the buffer versus temperature was found using the measured dimensions of the buffers, along with the measured temperature and the measured sound speeds of the buffers. Note that the measurement cell may be operated empty, to obtain the acoustic impedance of the buffer material using this approach. However, this was not performed in this work.

By performing the calibration in this manner, a semi-absolute calibration approach is introduced, in which the only acoustic parameter necessary to be measured is the buffer sound speed, in addition to the measured temperature. This means that the normal calibration approach of using the acoustic impedance of distilled water for obtaining the acoustic impedance of the buffer material is avoided, because it is known to suffer from dependency on the actual transmit waveform [18] to a larger extent than for the proposed calibration approach. This is believed to be due to using the same diffraction correction for different pulse lengths, for example.

## IV. SIGNAL PROCESSING

### A. Sound Speed

The sound speeds in the buffers and in the liquid can be found by use of the 2-way propagation time difference $\Delta t_{i,j}$ of the respective echo signals for the indicated medium $n = 1, 2, 3$, see Fig. 1. The index $i$ represents the local maximum and minimum voltage values of the time trace, where a total of $M$ such voltage extreme values are considered, and $j$ is the individual shot number (signal trace), out of a total number of $N$ shots to be averaged. The sound speed can be given as

$$c_{i,j} = \frac{2l_n}{\Delta t_{i,j} + \Delta t^{\text{diff}}}, \tag{5}$$

where $\Delta t^{\text{diff}}$ is the temporal correction due to diffraction. The averaged sound speed over a complete burst signal can be given as

$$c_j = \frac{1}{M} \sum_{i=1}^{M} c_{i,j} = \frac{1}{M} \sum_{i=1}^{M} \frac{2l_n}{\Delta t_{i,j} + \Delta t^{\text{diff}}}. \tag{6}$$

The sound speed averaged over $N$ shots can therefore be given as

$$c = \frac{1}{N} \sum_{j=1}^{N} c_j = \frac{1}{N \cdot M} \sum_{j=1}^{N} \sum_{i=1}^{M} c_{i,j}$$

$$= \frac{1}{N \cdot M} \sum_{j=1}^{N} \sum_{i=1}^{M} \frac{2l_n}{\Delta t_{i,j} + \Delta t^{\text{diff}}}. \tag{7}$$

From Fig. 1, it is assumed that the echo signals used in the calculation of the reflection coefficient are free from possible effects due to reverberation from the transducer internals, because the transducers are not involved in the reflection process. This applies throughout, except for the multiple buffer signals used in the measurement of the buffer sound speed. Also it should be noted that the sound speed of the receive buffer may be susceptible to interference effects, because the receive buffer multiple echo experience contributions from 2 wave paths of the same length, which are 1) multiple reflected in the transmit buffer before the signal traverses through to the receive transducer for detection, and 2) multiple reflected in the receive buffer before the signal gets detected by the receive transducer. Therefore, the buffer sound speed should preferably be measured by the transmit buffer multiple echoes alone along with the length of the buffer. By sequentially transmitting from both sides of the measuring cell, the sound speeds of both buffers were obtained. It should also be noted that the sound speed of the buffers and the liquid were measured simultaneously by signals from each transducer (transmitter and receiver), giving redundancy of the measured parameters.

### B. Amplitude Measurements

The reflection coefficient was calculated by 2 differing approaches, where each echo signal's amplitude $a(t)$ (time domain), or $A(f)$ (frequency domain), was processed according to a time domain approach and to a frequency domain integration approach, respectively. In the time domain approach, the peak-peak values used in obtaining the reflection coefficient may be prone to both wideband noise and to coherent noise. This approach has, however, the inherent benefit that it is not dependent on DC-offsets, as long as the offset is constant throughout the echo pulses considered.

Higuti and Adamowski [8] use a frequency domain integration approach as follows:

$$A_{k,j} = \int_{f_1}^{f_2} |A_{k,j}(f)| df, \ \ k = 1, 2, 3. \tag{8}$$

This treats the amplitude spectrum according to the $l^1$-norm. Here, the Fourier transformation pairs

$$
\begin{aligned}
a_{1,j}(t) &\leftrightarrow A_{1,j}(f) \\
a_{2,j}(t) &\leftrightarrow A_{2,j}(f) \\
a_{3,j}(t) &\leftrightarrow A_{3,j}(f)
\end{aligned}
\tag{9}
$$

reflect on the time domain and the frequency domain representations of the echo signals amplitudes. However, in this work, the amplitudes will be processed according to the $l^2$-norm as

$$
A_{k,j} = \sqrt{\int_{f_1}^{f_2} |A_{k,j}(f)|^2 \, df},
\tag{10}
$$

accentuating the dominant part of the frequency spectrums, making it easier to evaluate the effect of the upper frequency limit, $f_2$, as will be shown later. These frequency domain integration methods introduce a spectral averaging approach, reducing the effect of single-frequency interference in the echo signals.

Other methods exist, such as the frequency domain method as used by Adamowski *et al.* [6] where the reflection coefficient is found from the frequency content of a single bin. However, such an approach seems to have a high sensitivity to wideband noise [8]. Also, a time domain amplitude integral approach [19] may be used according to

$$
A_{k,j} = \int_{t_{1,j}}^{t_{2,j}} |\mathrm{env}[a_{k,j}(t)]| dt,
\tag{11}
$$

using distinct time information from the voltage maxima and minima in the echo signals as integration limits. However, this method was considered to be highly sensitive to DC-offsets in the echo signals and to waveform disturbance effects, because the integration is performed in the time domain with a duration determined by the transmitted burst length.

### C. Reflection Coefficient

For the time domain representation of the reflection coefficient, the peak-peak voltage over a given number of periods $p$ is needed, according to

$$
A_{k,j,p} = a_{k,j}(t_{p+}) - a_{k,j}(t_{p-}),
\tag{12}
$$

where $t_{p+}$ and $t_{p-}$ are the times for local maximum and minimum values of the time trace $a_{k,j}$ within period $p$. The reflection coefficient based on period $p$ of a single shot $R_{j,p}$ is calculated according to (1) and (2) for the ABC and for the R_echo12_12 method, respectively. The mean reflection coefficient based on a given number of periods is calculated as

$$
R_j = \frac{1}{P_2 - P_1 + 1} \sum_{p=P_1}^{P_2} R_{j,p}.
\tag{13}
$$

Thereafter, the mean reflection coefficient for a given number of shots is found as

$$
R = \frac{1}{N} \sum_{j=1}^{N} R_j.
\tag{14}
$$

For the frequency domain representation, the reflection coefficient is obtained by inserting (10) into (1) and (2), and finally averaging over the number of shots used through (14).

Because both transducers were used in the acquisition of the echo signals, an approach was assigned to ensure an equivalent importance of each transducer in the transmitting and in the receive operation. This was performed by using both transducers as transmitters in a sequential manner, where the measured sound speeds and the reflection coefficients as obtained using transmission from either side were averaged. Hence, an increased use of averaging and redundancy was introduced. The resulting density can be given by

$$
\rho_2 = \frac{\rho_1 \langle c_1 \rangle (1 + \langle R \rangle)}{\langle c_2 \rangle (1 - \langle R \rangle)},
\tag{15}
$$

where the terms in brackets means that they were averaged by considering the values as obtained by transmission from both sides.

### D. Least Squares Sense Cubic Spline Approximation

The calculation of sound speeds is described above. To obtain an increased vertical and temporal resolution, and at the same time avoid the possibility of nearby samples having the same voltage value due to the limited vertical resolution of a digitizer, a least squares sense cubic spline approximation was applied. The sound speeds in the buffers and in the sample were obtained by applying a threshold and a time gating on the echo signals. A third order least squares sense cubic spline approximation was used with equal weight given to each individual data point; 1500 splines were used on each time trace consisting of 2000 points, with a raw data time resolution of 17 ns. The processed time resolution from the cubic spline approximation used was 1 ns.

The effect of the cubic spline approximation can be illustrated by simulating the echo signals from a measurement cell with given input parameters, then performing the time and frequency domain processing to obtain the density. The synthetic input waveform used in the simulations is a causal Berlage wavelet of the form [20]

$$
g(t) = B \, t^m e^{-bt} \cos(2\pi f_0 t + \varphi_0) H(t),
\tag{16}
$$

where $B$ is a constant and $H(t)$ is the Heaviside function. The parameters used are $B = 0.5 \cdot 10^{15}$, $m = 2$, $b = 6 \cdot 10^6$, $f_0 = 6$ MHz, $\varphi_0 = -\pi/2$. The wavelet is given in Fig. 4.

The simulations were performed in the same manner as the measurements, using a time duration of 34 $\mu$s together with a time resolution of 17 ns, giving 2000 sampling
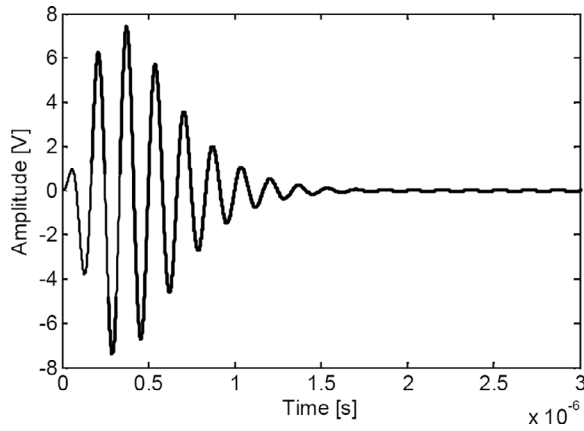
Fig. 4. Berlage wavelet as input to the simulation model of the acoustic measuring cell.
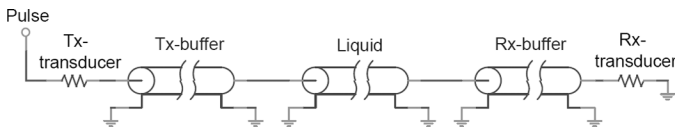


Fig. 5. Lossless *PSpice* simulation model of the acoustic measuring cell.

points. Simulations are performed by the time domain circuit simulator *PSpice* (Cadence Design Systems, Inc., San Jose, CA), as given in Fig. 5, obeying a lossless plane wave propagation. The simulated echo signals were exposed to finite vertical resolution according to

$$V_{\text{ADC}} = \text{int} \left( \frac{V_{\text{sample}} 2^{Q-1}}{V_{\text{max}}} \right) \frac{V_{\text{max}}}{2^{Q-1}}, \qquad (17)$$

where $V_{\text{ADC}}$ is the value of the voltage sample after given a finite vertical resolution, $V_{\text{max}}$ is the maximum voltage value in each echo signal in the absolute value sense, $V_{\text{sample}}$ is the individual voltage value of the sample, and $Q$ is the number of bits used. The simulation parameters are given in Table II, for the proposed measuring cell, see below. The used signal processing parameters are given in Table III. In Table IV and Table V the processed densities for the $R\_echo12\_12$ and the ABC method are given versus number of splines and vertical resolution used, for both the time domain and the frequency domain approaches.

Because 6 MHz represents the highest output frequency of the function generator used in burst mode, Table IV and Table V are expected to represent the worst-case characteristics of the frequency range used. The effect of the cubic spline approximation on the estimation of the liquid

### TABLE II
#### SIMULATION PARAMETERS OF THE ACOUSTIC MEASURING CELL.

| | $c$ [m/s] | $Z$ [$10^6$ kg/m$^2$s] | $l$ [$10^{-3}$ m] |
|---|---|---|---|
| Transducers | — | 2 | $\infty$ |
| Buffers | 6450 | 17 | 80 |
| Liquid | 1500 | 1.5 | 5.7 |

### TABLE III
#### SIGNAL PROCESSING PARAMETERS.

| Parameters | Value |
|---|---|
| # periods | 5 |
| Integration bandwidth | 0–10 MHz |
| Frequency resolution | $\approx$30.5 kHz |
| Norm | $l^2$ |
| Spline temporal resolution | 1 ns |

### TABLE IV
#### EFFECT OF THE CUBIC SPLINE APPROXIMATION ON THE LIQUID DENSITY FOR THE $R\_echo12\_12$ METHOD.

| | Density deviation [%] | | | | | |
|---|---|---|---|---|---|---|
| | Time domain | | | Frequency domain | | |
| # of splines | 8 bits | 10 bits | 12 bits | 8 bits | 10 bits | 12 bits |
| 500 | 3.84 | 3.66 | 3.68 | −0.77 | −0.90 | −0.93 |
| 1000 | 0.04 | −0.12 | −0.15 | −0.03 | 0.01 | −0.03 |
| 1500 | 0.14 | −0.06 | −0.02 | 0.05 | 0.02 | 0.00 |

In these tables, synthetic input data were used using a time resolution of 1 ns, and a frequency of 6 MHz.

and the buffer sound speeds were found to be negligible, using the synthetic input data. It was found that the frequency domain approach gives significantly less density deviation than the time domain approach. The variation in density using 10 to 12 bits and 1000 to 1500 splines for the $R\_echo12\_12$ method is ±0.03%, and for the ABC method it is within ±0.05% for the frequency domain approach.

#### E. Frequency Domain Signal Processing

The frequency domain signal processing chain can be described in the following steps:

1) Apply DC-offset correction $S_{DC}$ on the individual echo signals by measuring the average voltage value in a short time window just before the appearance of the first echo signal on each channel.
2) Apply a frequency independent amplitude diffraction correction factor $S^{\text{diff}}$ for each echo signal.
3) Multiply the individual echo signals by a Hanning window function $w(t)$ to reduce the spectral leakage. This was performed in a coherent fashion, so that the win-

### TABLE V
#### EFFECT OF THE CUBIC SPLINE APPROXIMATION ON THE LIQUID DENSITY FOR THE ABC METHOD.

| | Density deviation [%] | | | | | |
|---|---|---|---|---|---|---|
| | Time domain | | | Frequency domain | | |
| # of splines | 8 bits | 10 bits | 12 bits | 8 bits | 10 bits | 12 bits |
| 500 | 0.11 | −0.86 | −0.65 | −0.04 | −1.07 | −0.98 |
| 1000 | 0.03 | −0.66 | −0.42 | 0.65 | −0.04 | 0.02 |
| 1500 | 0.67 | −0.31 | −0.01 | 0.74 | −0.05 | 0.04 |

dow function was applied to the same relative point in all the echo signals. The placement of the window function moves throughout the bursts according to which periods are used in the signal processing.

4) Apply zero padding for each echo until a desired frequency resolution was achieved, and thereafter perform the FFT-operation.

5) Integrate the individual frequency spectrums by the triangular method according to the given norm so that the frequency domain reflection coefficient was obtained.

These steps can be further described theoretically according to

$$a_{k,j}(t) = [s(t) - S_{DC}] \cdot S^{\text{diff}} \cdot w(t - t_w), \qquad (18)$$

where $s(t)$ is the cubic spline approximation of the sampled trace, and $a_{k,j}(t)$ expresses the resulting time domain signal after exposure to the window function, the DC-offset correction, and the amplitude diffraction correction; $t_w$ is the corresponding delay of the window function. By using the Fourier transformation pairs

$$\begin{aligned} w(t) &\leftrightarrow W(f) \\ s(t) - S_{DC} &\leftrightarrow S(f), \end{aligned} \qquad (19)$$

the frequency domain description is obtained according to

$$A_{k,j}(f) = S^{\text{diff}} \cdot S(f) * W(f)e^{-j2\pi f t_t}, \qquad (20)$$

with $*$ describing the convolution operator. Then, the resulting frequency domain integration amplitudes can be obtained according to (10).

For the measurement of the reflection coefficient to be performed in a comparable fashion between the time domain and the frequency domain approaches, an integer number of periods in the bursts was used at the processing stage. This is a necessary condition for the time domain approach as it uses peak-to-peak values, because otherwise DC-offsets would contribute, but for the frequency domain approach a single half-period in each echo signal could be used for the calculation of the reflection coefficient. This behavior is better explained in Fig. 6 using only one period of processing for the burst waveform shown.

For each centration of the window function (see Fig. 6), a value for the reflection coefficient is obtained. In practice, the reflection coefficients originating from various voltage extreme values in the bursts are averaged. The placement of the window function dictates its width limited in one end by the start of the acquisition window and in the other end by not extending across nearby echo signals. The width also determines the spectral characteristic of the echo signals considered, with a wide window giving a band pass behavior, and a narrow width giving a low pass behavior, effectively weighting the frequency range differently.

The effect of the upper frequency limit on the norm used, see (8) and (10), can be visualized according to Fig. 7, where the processed density versus frequency is given based on a synthetic echo sequence using a 5 period,
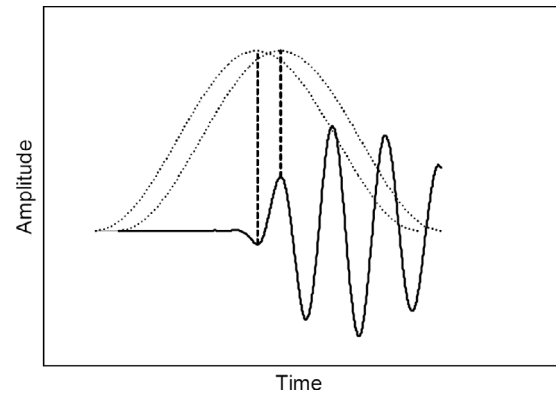


Fig. 6. An example of the use of an integer number of periods in the transmit burst for the calculation of the reflection coefficient. The 2 window functions are centered at the 2 first voltage extreme values.
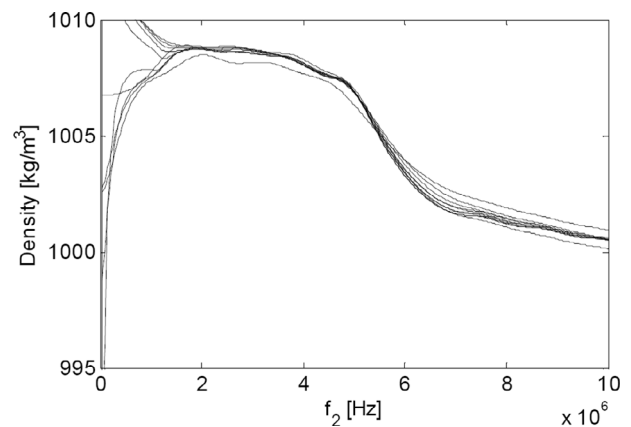


Fig. 7. Typical processed density versus the upper frequency limit $f_2$ (cf. (8)), using the $l^1$-norm using synthetic input data. The lower frequency limit was equal to zero. The density reference value is 1000 kg/m$^3$. The different curves represent density as obtained from the various voltage extreme values in the bursts.

6 MHz burst for the $l^1$-norm, with the corresponding result using the $l^2$-norm shown in Fig. 8. In these figures, a processed density curve versus the upper frequency limit is given for each of the voltage extreme values in the burst. The lower frequency limit was set equal to zero.

It is seen that the $l^2$-norm has a flatter characteristic versus upper frequency limit above the transmit frequency of the burst than the $l^1$-norm, making it easier to set an upper frequency limit in the signal processing. The choice of the lower frequency limit was found through simulations not to influence the processed density.

The use of the triangular integration method instead of the standard Matlab (The MathWorks, Natick, MA) quadrature integration routine greatly speeded up the processing. Also, the effect of the frequency resolution using the triangular integration routine is seen in Fig. 9 to be negligible in a very wide range while only a minor difference in processing speed was found.

The effect of using one period of the Berlage wavelet throughout the pulse is given in Fig. 10, where using the first period shows a significantly increased deviation from
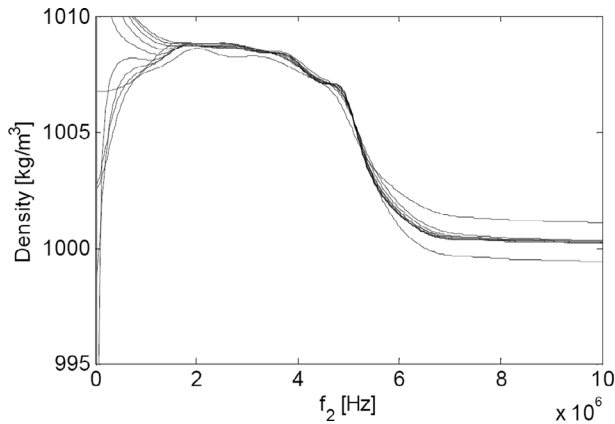
Fig. 8. Typical processed density versus the upper frequency limit $f_2$ (cf. (10)), using the $l^2$-norm using synthetic input data. The lower frequency limit was equal to zero. The density reference value is 1000 kg/m$^3$. The different curves represent density as obtained from the various voltage extreme values in the bursts.



Fig. 10. Processed density based on synthetic input data for the $R\_echo12\_12$ method and for the ABC method, using both a time domain and a frequency domain signal processing. The effect of using one period of the Berlage wavelet throughout the pulse is given. The density reference value is 1000 kg/m$^3$.
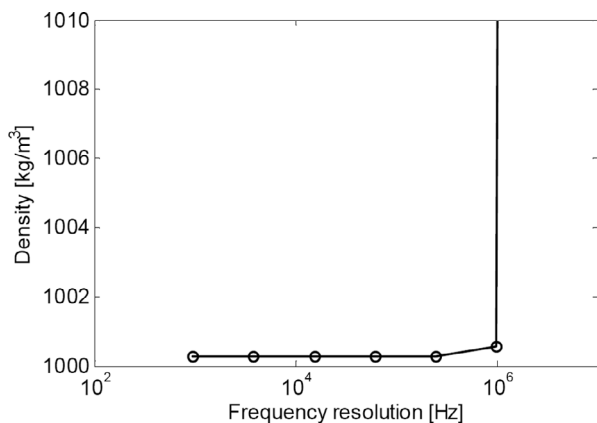


Fig. 9. Typical processed density versus frequency resolution using synthetic input data and the frequency domain processing approach. The density reference value is 1000 kg/m$^3$.

the reference value compared with the rest of the pulse. The reason for this behavior must be attributed to the reflection coefficient, because the sound speeds shows negligible deviation throughout the pulse. Due to a reduced effective bit resolution of the first period of the wavelet, the reflection coefficient suffers an increased uncertainty of the first period compared with the rest of the pulse, as is evident from Fig. 4. This behavior has been verified also against experimental data, and as a consequence, the first period in the pulse was ignored at the processing stage. The time domain processing is seen to yield significantly increased deviations from the reference value as compared with the frequency domain processing.

### F. Diffraction Correction

To account for the beam spreading in the buffers and in the sample liquid, a single-frequency diffraction correction method was used, based on the carrier frequency of the signal. The exact Williams integral expression [21] is used for
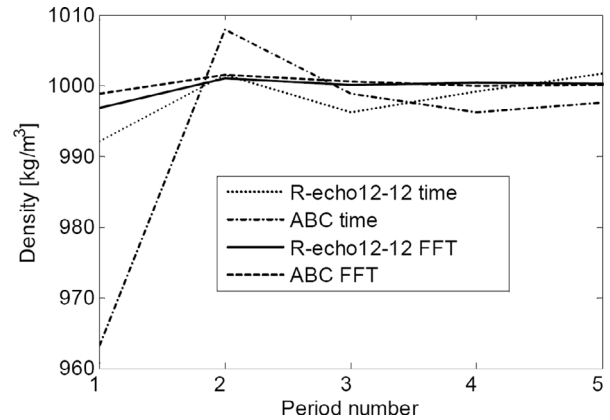
the calculation of diffraction in an isotropic and homogeneous lossless medium placed between 2 circular transducers of the same diameter with an axially concentric alignment. Continuous waves are assumed in this approach. Because several echo signals that have propagated different distances and through different mediums are used, the total propagation length was obtained using the Papadakis method [22], which is more fully described in [23], [24].

### V. MECHANICAL AND DIMENSIONAL DESIGN

#### A. Buffer Material

The acoustic impedance of the buffer material is an important parameter for determining the sensitivity of the measurement system. A low acoustic impedance material such as Perspex gives a high sensitivity due to better impedance matching against liquids, but may suffer from robustness and protection against aggressive liquids. A high acoustic impedance buffer such as stainless steel gives a low sensitivity. In this work, an aluminum quality 6082-T6 was used for the evaluation of the measurement principle due to the easy manufacture and because alternative materials with matching acoustical parameters are available [25]. These include the workable ceramic material Zerodur and the quartz glass, because they possess significantly more robust behavior than aluminum when exposed to different liquids.

#### B. Wave Propagation in Solids

A high temporal resolution for the measurement of sound speeds along with a high bit resolution of the echo signals is required to represent the measured signals as well as possible. This is obtained by avoiding interfering signals. To be able to achieve the maximum purity signals sought for, the following well-known wave-propagation effects in solids [26] must be accounted for: compression plane wave,
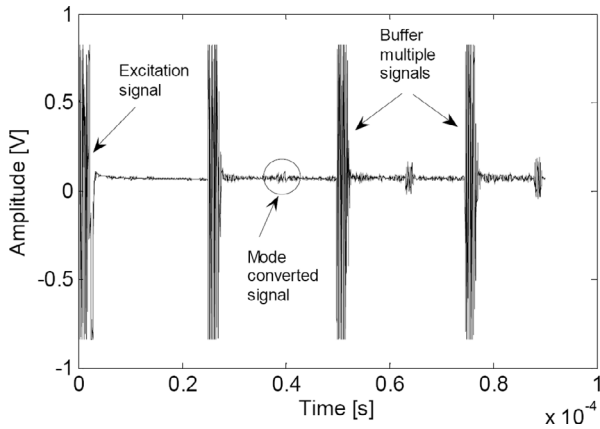
Fig. 11. Experimental demonstration of the mode converting nature as observed on the Tx-transducer.

TABLE VI

ACOUSTIC CHARACTERIZATION OF THE BUFFER MATERIAL AT ROOM TEMPERATURE. A FREQUENCY OF 5 MHz WAS USED.

| $c_1$ [m/s] | $c_{1s}$ [m/s] | $\nu$ | $E$ [GPa] |
|---|---|---|---|
| 6450 | 3085 | 0.35 | 70 |

compression edge wave, and shear edge wave. These waves get mode converted at interfaces where a solid meets a solid or a fluid. An example of the mode converted echo signals for an empty (air-filled) measurement cell of the dimensions given in Table VII is shown in Fig. 11, in which the switching arrangement was not used. Interference with such signals should be avoided.

### C. Acoustic Characterization of the Buffer

By measuring the compressional and the shear wave sound speeds in the buffer ($c_1$ and $c_{1s}$, respectively) using the arrival times of the echo signals from Fig. 11, the Poisson's ratio $\nu$ may be obtained from

$$\nu = \frac{1}{2} \frac{c_1^2 - 2c_{1s}^2}{c_1^2 - c_{1s}^2}. \quad (21)$$

The Poisson's ratio, in combination with either the compressional or the shear wave sound speeds in the buffer, gives the Young's modulus ($E$) for the buffer, assuming the density is known, e.g., from Table I. Measured results are given in Table VI for a circular buffer with a length of 80 mm and a diameter of 205 mm, which are in reasonable agreement with literature values [27] for the Poisson's ratio and the Young's modulus for this material. The shear wave sound speed is found from

$$c_{1s} = \frac{l_1}{t_{\text{mode}} - l_1/c_1}, \quad (22)$$

where $t_{\text{mode}}$ is the time of arrival of the first mode converted echo signal relative to the start of the transmit signal.

After having acoustically characterized the buffer material, one can approach the process of obtaining the optimum dimensions of the measurement cell.

### D. Dimensional Considerations

To be able to obtain maximum purity signals from a measuring cell according to the proposed measuring principle, the following dimensional considerations were identified as necessary:

1) None of the liquid echoes shall be overlapping.
2) The liquid echo signals involved for the various methods shall be detected *before* the multiple buffer echo signal is detected.
3) The transducer rim generated shear wave, which gets mode converted and reflected from the transmit buffer-liquid interface as a compressional wave, shall not interfere with the liquid echoes, arriving *after* the receipt of the last liquid echo to be used, which is $A_2$ for the $R\_echo12\_12$ method, and $A_3$ for the ABC method.
4) The transducer rim generated compressional wave burst reflected at the cylindrical end at the corner of the buffer shall return to the transmit transducer *after* the receipt of the last echo signal used for obtaining the reflection coefficient.

The equations describing these characteristics can be given as

$$l_2 > \frac{c_2 t_{\text{burst}}}{2} \quad (23)$$

for the liquid echoes being nonoverlapping, where $t_{\text{burst}}$ is the combined duration of the transmit burst and the transducer ring-down. For placing the multiple buffer echo signal after the liquid echoes $A_2$ and $A_3$, respectively, it is found that

$$l_2 < \frac{c_2}{2} \left( \frac{2l_1}{c_1} - t_{\text{burst}} \right) \quad (24)$$

is relevant for the $R\_echo12\_12$ method, and that

$$l_2 < \frac{c_2}{4} \left( \frac{2l_1}{c_1} - t_{\text{burst}} \right) \quad (25)$$

is relevant for the ABC method. For the mode converted echo signal from the buffer-liquid interface to be situated after the $A_2$ echo signal, the following constraint exists:

$$l_2 < \frac{c_2}{2} \left[ l_1 \left( \frac{1}{c_{1s}} - \frac{1}{c_1} \right) - t_{\text{burst}} \right], \quad (26)$$

where the shear wave sound speed in the buffers is given as

$$c_{1s} = \sqrt{\frac{\mu}{\rho}}, \quad (27)$$

and with the shear modulus $\mu$ given as a function of the Young's modulus and the Poisson's ratio as

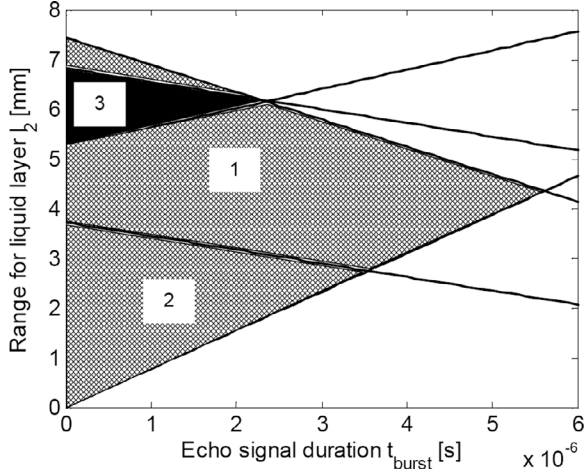$$\mu = \frac{E}{2(1+\nu)}. \quad (28)$$

Fig. 12. Allowed range of liquid thickness versus signal duration for a range of the liquid sound speed of 1100–1550 m/s. The identified regions are described in the text.
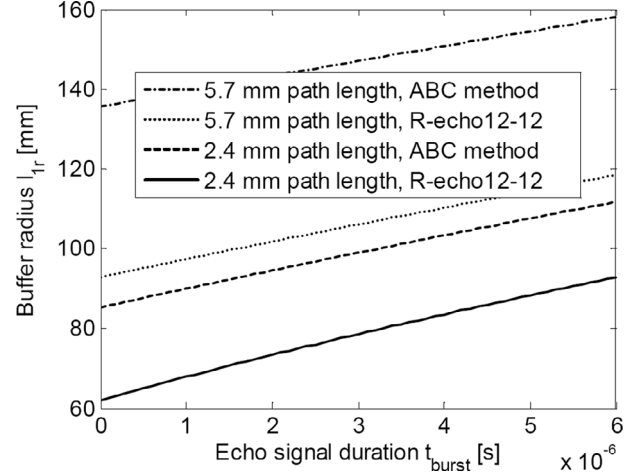


Fig. 13. Range of minimum buffer radius versus echo signal duration for a range of liquid sound speed of 1100–1550 m/s.

For the mode converted echo signal to be situated after the $A_3$ echo signal, it is found that

$$l_2 < \frac{c_2}{4}\left[l_1\left(\frac{1}{c_{1s}} - \frac{1}{c_1}\right) - t_{burst}\right]. \qquad (29)$$

By accounting for considerations 1 through 3 above, the combined allowed range for the liquid layer thickness is given in Fig. 12. There, a range of liquid sound speed of 1100 to 1550 m/s was assumed. This range covers pure water to a temperature of approximately 50°C, and in the lower range it covers most hydrocarbons of *n*-alkanes, 1-alkanes, and naphthenes [28], except at elevated temperatures, and silicone oils, which typically have lower sound speeds [29]. In Fig. 12, 3 regions can be identified, with the triangular region 1 covering all of the hatched area corresponding to the $R\_echo12\_12$ method. Region 2 corresponds to the ABC method, assuming the $A_3$ signal to appear before the mode-converted signal. Region 3 corresponds to the ABC method limited in the lower range by the mode-converted signal to appear before the $A_3$ signal, and in the upper range by the $A_3$ signal to appear before the multiple-buffer signal. From this, the $R\_echo12\_12$ method is seen to be able to cover a much larger range for the liquid layer and also to use an increased duration of the transmit signal, as compared with the ABC method.

In this work, 2 measuring cells were manufactured using the same buffers, but with different lengths of the liquid chambers. These lengths were based on the allowed liquid layer thicknesses from Fig. 12 for the ABC method. The liquid path lengths chosen were approximately 2.4 mm and 5.7 mm, to use the maximum signal duration.

The minimum radius of the buffers to receive the $A_2$ echo signal before the signal transmitted from the rim of the transducer to the corner of the buffer and reflected as a compressional wave is given by

$$l_{1r} > R_{TRD} + \sqrt{\left[\frac{c_1}{2}\left(2\frac{l_1}{c_1} + 2\frac{l_2}{c_2} + t_{burst}\right)\right]^2 - l_1^2}, \qquad (30)$$

TABLE VII
DIMENSIONS FOR THE MEASURING CELL.

|        | Diameter [mm] | Length [mm]   |
|--------|---------------|---------------|
| Buffer | 205           | 80            |
| Liquid | 107           | 2.4 and 5.7   |

where $l_{1r}$ is the buffer radius and $R_{TRD}$ is the radius of the transducer used. Assuming that the $A_3$ echo signal arrives before the signal transmitted from the rim of the transducer to the corner of the buffer and reflected, the relationship is given by

$$l_{1r} > R_{TRD} + \sqrt{\left[\frac{c_1}{2}\left(2\frac{l_1}{c_1} + 4\frac{l_2}{c_2} + t_{burst}\right)\right]^2 - l_1^2}. \qquad (31)$$

The range of allowed buffer radius versus echo signal duration is shown in Fig. 13 for liquid layer thicknesses of 2.4 mm and 5.7 mm, and assuming a transducer radius of 12.5 mm. To limit the buffer dimensions, it was decided to use a radius of 102.5 mm, which corresponds to the use of both methods for the 2.4 mm liquid path length, and the 5.7 mm path length for the $R\_echo12\_12$ method, complying with a signal duration of about 3 $\mu$s. It is also seen that the use of the $R\_echo12\_12$ method makes it possible to reduce the size of the buffers significantly as compared with the ABC method.

*E. Measuring Cell*

These figures, together with knowledge of the obtainable echo signal duration for a given excitation signal, led to the dimensions given in Table VII for the measurement cell manufacture. The diameter of the liquid sample chamber was 107 mm. No influence of the insertion of the thermistor probe into the liquid was found, probably due to the highly directional sound beam.
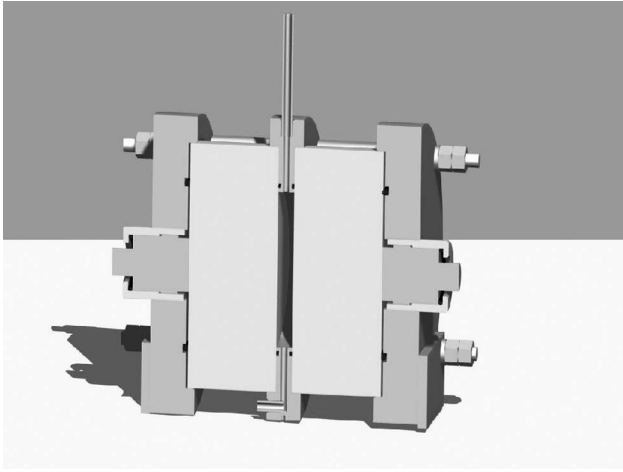
Fig. 14. Cross-sectional view of the measurement cell; NB: not to scale.

| Viscosity standard | Shear viscosity [mPa·s] | Kinematic viscosity [mm²/s] | Liquid density [kg/m³] |
|---|---|---|---|
| N4 | 5.242 | 6.668 | 786.2 |
| N7.5 | 11.37 | 14.19 | 800.9 |
| N35 | 74.93 | 86.38 | 867.5 |
| N100 | 282.8 | 320.6 | 881.9 |

## VI. EXPERIMENTAL RESULTS

### A. Liquids to Be Measured

Several researchers have performed measurements on liquids that span a very large range in densities, ranging from approximately 750 kg/m³ for alcohols/gasoline to 1260 kg/m³ for glycerin [8], [30]. The density of oils, however, is known to span a much smaller range, because the lowest density hydrocarbon is pentane with a density of approximately 670 kg/m³, and a high-density hydrocarbon is typically a heavy crude oil having a density of approximately 920 kg/m³ [31]. Most often, acoustic measurements are compared with reference measurements performed with a calibrated pycnometer [8], [30], giving a great flexibility in which to measure liquid. Such pycnometers typically have a relative uncertainty of ±0.1%.

To avoid the uncertainty of the pycnometer, it was found desirable to use liquids with a calibrated density across a certain temperature range. Cannon Instrument Company, State College, PA, [32] supplies certified reference standards from which some general-purpose viscosity standards were used in this work to cover a broad range of shear viscosities. The viscosity standards were supplied in 500 mL bottles, with a density uncertainty of ±0.1 kg/m³. The parameters of the Cannon viscosity standards that were used are given in Table VIII. No information about the standards' sound speed or attenuation characteristics were given by the vendor or found in the literature.

The density of distilled water versus temperature is known to have a negligible maximum uncertainty of 0.17 ppm in the temperature range of 0 to 41°C [33].

### B. Results

Density measurement results for the different liquids are given in Tables IX to XI, with extended measurement results given in [34]. All the measurements were performed at a temperature of 27.44 ± 0.04°C. As an example of the specific measurement results, the ABC method at 6 MHz using the 5.7 mm cell is given in Table IX, using a frequency domain signal processing. There, the N100 oil is seen to have a significant deviation from the reference value, exceeding 4%. The reason for this large deviation is attributed to the significant waveform distortion observed

A schematic cross-sectional view of the measurement cell is given in Fig. 14. The assembly of the cell was performed by using some stainless steel spacers keeping the liquid path length fixed. The measurement cell was tightened by a torque wrench to a torque of 28 Nm. The transducers were fitted snugly into their housings, which were screwed onto the solid end caps by hand so that the transducers got in close contact with the aluminum buffers. A *thin* layer of Krautkrämer ZGT acoustic coupling paste was inserted on the transducer fronts. The twisting of the transducers against the buffers ensured a uniform thickness of the coupling paste and improved the acoustic coupling.

The liquid filling of the measuring cell was performed for the least viscous liquids by using a syringe in a way that let the liquid pour freely without introducing mixing of the liquid and air in a significant manner. For the most viscous liquid (Cannon N100) a different procedure was necessary. Then, one of the buffers and the measuring chamber were mounted together with the surface of the buffer in a horizontal position. The liquid was then poured directly onto the buffer until it nearly reached the top of the measuring chamber, taking precautions not to fill the liquid inlet. Then, on the complete mounting of the cell, the air inside the chamber was pressed out from the liquid inlet without being mixed with the liquid.

The temperature was kept constant at least 30 min after thermal equilibrium was obtained, before measurements were acquired. Also, the thermostat-regulated water bath includes a stirrer keeping a constant water circulation around the measurement cell.

### F. Nonparallelism

The transducer and liquid contact faces of the buffers were lapped and found to be parallel to within 0.01 mm across the diameter, due to the mechanical design and manufacture of the measurement cell, indicating the negligible effect of nonparallelism in this measurement cell.

## TABLE IX
Measurements on Distilled Water and Cannon Viscosity Standards Using the 5.7 mm Measuring Cell for the ABC Method at 6 MHz, Using a Frequency Domain Signal Processing.

| Liquid | Reference density [kg/m³] | Measured density [kg/m³] | Relative difference [%] |
|---|---|---|---|
| Distilled water | 996.40 | 996.24 | −0.02 |
| N4 | 781.20 | 779.81 | −0.18 |
| N7.5 | 796.02 | 797.79 | 0.22 |
| N35 | 862.73 | 856.33 | −0.74 |
| N100 | 877.32 | 837.82 | −4.50 |

## TABLE X
Summary of Density Measurement Results Using the 5.7 mm Measuring Cell.

| Method | 4 MHz Mean dev. [%] | 4 MHz 0.5 · Span [%] | 5 MHz Mean dev. [%] | 5 MHz 0.5 · Span [%] | 6 MHz Mean dev. [%] | 6 MHz 0.5 · Span [%] |
|---|---|---|---|---|---|---|
| $R\_echo12\_12$ time domain | −0.35 | 0.06 | −0.14 | 0.15 | −0.14 | 0.19 |
| $R\_echo12\_12$ freq. domain | −0.44 | 0.09 | −0.28 | 0.14 | −0.34 | 0.31 |
| ABC time domain | −0.17 | 0.14 | 0.05 | 0.19 | 0.05 | 0.41 |
| ABC freq. domain | −0.32 | 0.17 | −0.13 | 0.15 | −0.18 | 0.48 |

The liquids used were distilled water, and the N4, N7.5, and the N35 viscosity standards. The N100 oil was excluded due to the mentioned waveform distortion characteristics.

## TABLE XI
Summary of Density Measurement Results Using the 2.4 mm Measuring Cell.

| Method | 4 MHz Mean dev. [%] | 4 MHz 0.5 · Span [%] | 5 MHz Mean dev. [%] | 5 MHz 0.5 · Span [%] | 6 MHz Mean dev. [%] | 6 MHz 0.5 · Span [%] |
|---|---|---|---|---|---|---|
| $R\_echo12\_12$ time domain | −0.40 | 0.39 | −0.16 | 0.12 | −0.06 | 0.49 |
| $R\_echo12\_12$ freq. domain | −0.51 | 0.15 | −0.30 | 0.09 | −0.37 | 0.56 |
| ABC time domain | −0.01 | 0.67 | −0.09 | 0.22 | 0.19 | 0.68 |
| ABC freq. domain | −0.31 | 0.22 | −0.17 | 0.12 | −0.09 | 0.64 |

The liquids used were distilled water, and the N4, N7.5, N35, and the N100 viscosity standards.

[34]. The N100 oil did not show any significant waveform distortion using the 2.4 mm measuring cell. This is illustrated by the attenuation of the $A_3^*$ signal, which is about 10 dB in the 2.4 mm cell at 6 MHz and about 12 dB at 4 MHz using the 5.7 mm cell [34].

In Tables X and XI the summary results using different frequencies and different measuring methods are given for the 5.7 mm and for the 2.4 mm measuring cell, respectively. Each frequency has 2 columns. The first gives the mean deviation in percent over the 5 liquids presented in Table IX from the density reference values according to

$$\text{Mean deviation} = \frac{1}{5}\sum_{i=1}^{5}\left(100\frac{\rho_i - \rho_{\text{ref},i}}{\rho_{\text{ref},i}}\right). \quad (32)$$

The second column gives half the span in percent between the maximum and the minimum deviation from the reference values, where the span in percent is defined by

$$\text{Span} = \max\left(100\frac{\rho_i - \rho_{\text{ref},i}}{\rho_{\text{ref},i}}\right) - \min\left(100\frac{\rho_i - \rho_{\text{ref},i}}{\rho_{\text{ref},i}}\right). \quad (33)$$

This way, the second column can be compared more easily with predicted uncertainties. In Table X, the N100 oil was excluded due to the mentioned waveform distortion characteristics.

For both measuring cells, it was in general found that the systematic deviation from reference values was smaller for the ABC method than for the $R\_echo12\_12$ method. A possible explanation for this behavior may be due to diffraction correction, because the ABC method uses only one transducer, whereas the $R\_echo12\_12$ method uses 2 transducers. Because the transducers cannot be expected to have identical sound fields, the added error on the use of identical diffraction correction on different transducers is believed to be responsible for such a behavior. The effect of such a systematic deviation may be reduced by applying a suitable zero-point correction, which may be performed by subtracting the obtained systematic deviation based on measurements on several liquids from the actual measured density for a given liquid.

The measurement span of the density as compared with the respective reference density was found to be within ±0.15% for the $R\_echo12\_12$ method for both measuring cells at 5 MHz, for both time and frequency processing using liquids with a wide range of shear viscosities. The span using the ABC method was larger than for the $R\_echo12\_12$ method. This will be seen to be in accordance with the uncertainty analysis in Section VII.

## VII. Uncertainty Analysis

The uncertainty analysis is based on the same formalism as given in [14] for the relative amplitude approach, but extended to deal with liquid density instead of reflection coefficient only. Here, the effects of bit resolution and time resolution are studied. The partial derivative approach is
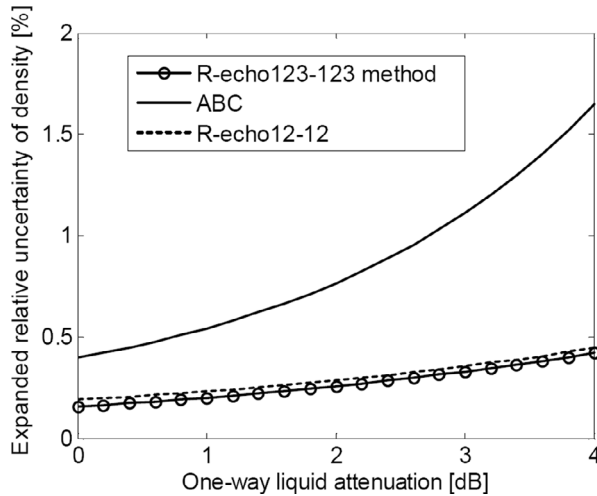
Fig. 15. Simulated effect of liquid attenuation on the expanded relative uncertainty of the density. A resolution of 12 bits was used. The noise characteristics were ignored.
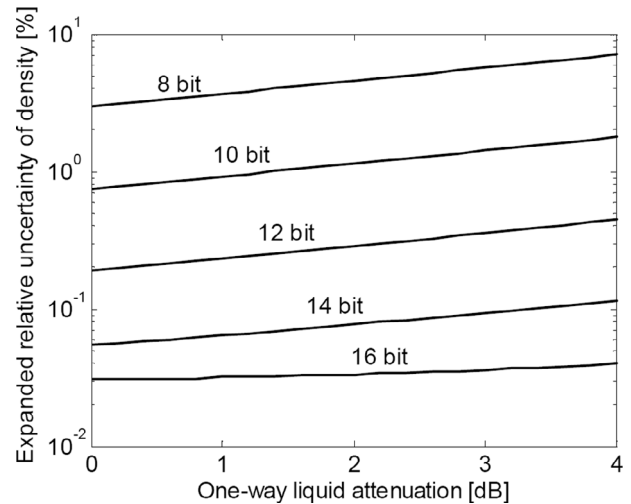


Fig. 16. Simulated effect of bit resolution on the expanded relative uncertainty characteristics of the $R\_echo12\_12$ method versus liquid attenuation. The noise characteristics were ignored.

used to obtain the expanded relative uncertainty of the density as given in (4) according to

$$k^2 \left[ \frac{u(\rho_2)}{\rho_2} \right]^2 = \frac{k^2}{\rho_2^2} \sum_{i=1}^{R} \left( \frac{\partial \rho_2}{\partial x_i} u(x_i) \right)^2 , \qquad (34)$$

where $u$ indicates the standard uncertainty, and $x$ indicates the mutual uncorrelated variable on which the liquid density depends. A coverage factor $k = 2$ for a 95% confidence interval was used.

For the amplitudes behind the reflection coefficient, a rectangular distribution probability function of the quantization process was assumed [14]. To study the uncertainty characteristics, a relative uncertainty of 0.01% was assigned as an example to both the buffer and the liquid sound speeds, based on using a time resolution of 1 ns from the cubic spline approximation. This is not the total uncertainty, but an effect due to time resolution. The density uncertainty of the buffer was neglected in the following simulations, due to its precisely known value. The simulation parameters of the buffer and the liquid are given in Table II.

The expanded relative uncertainty of liquid density versus the liquid attenuation is given in Fig. 15 assuming a resolution of 12 bits. The expanded relative uncertainty of the $R\_echo12\_12$ method is seen to be close to the $R\_echo123\_123$ method given in [14]. It should be mentioned that the implementation of the $R\_echo123\_123$ method depends on the attenuation of the liquid. Therefore, it is not a straightforward method to use, from a practical point of view.

The expanded relative uncertainty of the ABC method is seen to increase as the attenuation increases at a faster rate than the $R\_echo12\_12$ method and to also have about double the uncertainty at very low attenuation. The effect of varying bit resolution for the $R\_echo12\_12$ method is given in Fig. 16, using a range of 8 to 16 bits. For 12 bits, an expanded relative uncertainty of about 0.2% can
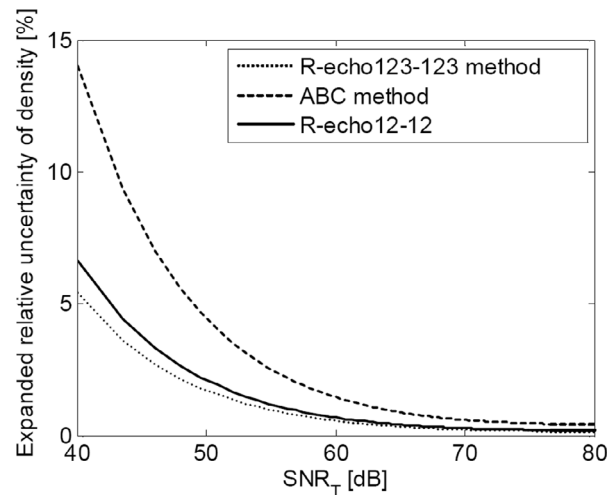


Fig. 17. Simulated effect of SNR of the first echo signal on each transducer on expanded relative uncertainty of the density. Zero liquid attenuation was assumed, together with a resolution of 12 bits. Aluminum buffers were assumed and a liquid sound speed of 1500 m/s.

be expected, compared with about 0.06% using 14 bits, and 0.03% using a resolution of 16 bits, assuming a low attenuation.

In the results presented here, the effect of noise was ignored.

The effect of noise in addition to bit resolution and time resolution will now be studied. By assigning the same SNR of the first echo signal on each transducer, the expanded relative uncertainty of density versus the SNR ratio can be given as in Fig. 17, assuming a random noise characteristic. Because the amplitudes of the different signals are widely different, while the random noise characteristic is rather constant throughout the echo signals, a single number of SNR cannot be given. Using measurements performed on distilled water and on the N100 oil, the estimated SNR for each echo signal are given in Table XII for the 5.7 mm

TABLE XII
MEASURED SNR FOR THE VARIOUS ECHO SIGNALS USING PURE
WATER AND THE N100 OIL.

| Liquid | Estimated SNR [dB] | | | | | |
|---|---|---|---|---|---|---|
| | $A_1$ | $A_2$ | $A_3$ | $A_1^*$ | $A_2^*$ | $A_3^*$ |
| Water | 62 | 51 | 47 | 63 | 60 | 57 |
| N100 | 62 | 43 | 34 | 67 | 57 | 48 |

A frequency of 5 MHz was used along with an averaging factor of 256, using the 5.7 mm measuring cell.
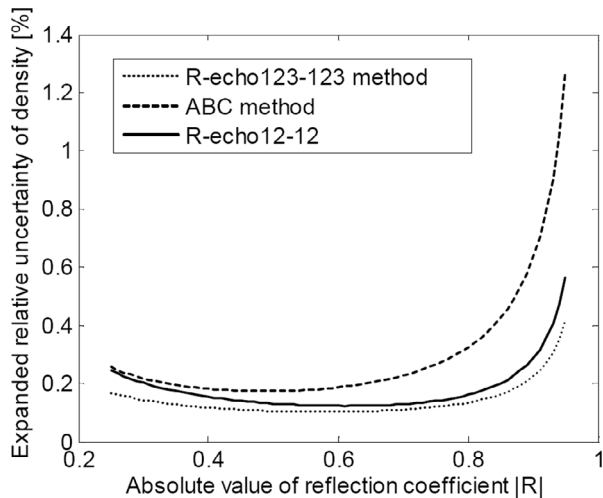


Fig. 18. Simulated effect of $|R|$ on the expanded relative uncertainty of the liquid density. Zero attenuation was assumed along with 12 bits resolution. The noise characteristics were ignored, and aluminum buffers were assumed.

path length measurement cell. The measured SNR in Table XII was obtained by noting the peak-to-peak values of the signals and the random noise, taking care to avoid systematic noise contributions such as mode conversion and direct electrical cross feed between the transmit and the receive channel. From Table XII the improved SNR of the $R\_echo12\_12$ method can be seen by referring to the specific amplitude ratios given in (1) and (2).

The expanded relative uncertainty of density versus $|R|$ is given in Fig. 18. An aluminum buffer was assumed together with a fixed sound speed of the liquid of 1500 m/s. The noise characteristics were ignored. For water, $|R|$ is about 0.83, whereas for typical oils, $|R|$ is about 0.90, and the expanded relative uncertainty is seen to be higher for oils than for water, due to the increased acoustic mismatch of the acoustic impedances. The $R\_echo12\_12$ method is seen to leap from the ABC method at low values of $|R|$ and approach the lowest uncertainty and case-dependent $R\_echo123\_123$ method. The $R\_echo12\_12$ method is therefore seen to possess close to optimum behavior at a wide range of $|R|$. This is in contrast to the ABC method.

## VIII. DISCUSSION

As seen in Fig. 10, including the first period of the waveforms in the signal processing may give large errors, par-

ticularly when using a time domain processing. This has also been observed experimentally where density errors approaching 15% were found using only the first period. This error was found in some cases to be greatly different when transmitting from one side of the cell compared with transmitting from the other end. By avoiding the first period in the signal processing, more equal characteristics were obtained when transmitting from both sides of the measuring cells. This also led to a more proper use of the single-frequency diffraction correction, because part of the transient waveform was avoided.

Using the 5 MHz center frequency of the transducer, a measurement span within ±0.15% was obtained for a wide range of liquid viscosities. This was obtained for both measurement cells and for both the time and the frequency domain processing schemes. Also, by using a zero-point correction factor, the systematic deviation could be reduced for a specific measurement method and signal processing chosen.

## IX. CONCLUSIONS

A new method for measuring liquid density acoustically using a buffer rod approach was given, with improved uncertainty characteristics relative to the ABC method. The new method facilitates the use of a thicker liquid layer without suffering from interference due to mode conversion and was shown to be significantly less prone to the effect of liquid attenuation. An improved frequency domain integration signal processing approach was suggested using the $l^2$-norm, making it easier to set the processing parameters correctly. Using liquids with a wide viscosity range, the measured density span was within ±0.15%. The main achievements are believed to be the experimental verification of the proposed $R\_echo12\_12$ method in comparison with the ABC method.

## REFERENCES

[1] D. J. McClements and P. Fairly, "Ultrasonic pulse echo reflectometer," *Ultrasonics*, vol. 29, pp. 58–62, 1991.

[2] D. J. McClements and P. Fairly, "Frequency scanning ultrasonic pulse echo reflectometer," *Ultrasonics*, vol. 30, pp. 403–405, 1992.

[3] J. Kushibiki, N. Akashi, T. Sannomiya, N. Chubachi, and F. Dunn, "VHF/UHF range bioultrasonic spectroscopy system and method," *IEEE Trans. Ultrason., Ferroelect., Freq. Contr.*, vol. 42, no. 6, pp. 1028–1039, Nov. 1995.

[4] E. P. Papadakis, "Buffer-rod system for ultrasonic attenuation measurements," *J. Acoust. Soc. Amer.*, vol. 44, no. 5, pp. 1437–1441, 1968.

[5] A. Püttmer, P. Hauptmann, and B. Henning, "Ultrasonic density sensor for liquids," *IEEE Trans. Ultrason., Ferroelect., Freq. Contr.*, vol. 47, no. 1, pp. 85–92, Jan. 2000.

[6] J. C. Adamowski, F. Buiochi, C. Simon, E. C. N. Silva, and R. A. Sigelmann, "Ultrasonic measurement of density of liquids," *J. Acoust. Soc. Amer.*, vol. 97, no. 1, pp. 354–361, Jan. 1995.

[7] J. C. Adamowski, F. Buiochi, and R. A. Sigelmann, "Ultrasonic measurement of density of liquids flowing in tubes," *IEEE Trans. Ultrason., Ferroelect., Freq. Contr.*, vol. 45, no. 1, pp. 48–56, Jan. 1998.

[8] R. T. Higuti and J. C. Adamowski, "Ultrasonic densitometer using a multiple reflection technique," *IEEE Trans. Ultrason., Ferroelect., Freq. Contr.*, vol. 49, no. 9, pp. 1260–1268, Sep. 2002.

[9] M. Hirnschrodt, A. von Jena, T. Vontz, B. Fischer, R. Lerch, and H. Meixner, "Time domain evaluation of resonance antireflection (RAR) signals for ultrasonic density measurement," *IEEE Trans. Ultrason., Ferroelect., Freq. Contr.*, vol. 47, no. 6, pp. 1530–1539, Nov. 2000.

[10] M. Hirnschrodt, A. von Jena, T. Vontz, B. Fischer, and R. Lerch, "Ultrasonic characterization of liquids using resonance antireflection," *Ultrasonics*, vol. 38, pp. 200–205, 2000.

[11] J. Delsing, "On ultrasonic flow meters. Investigations and improvements of the sing-around flow meter," Ph.D. dissertation, Lund Institute of Technology, Lund, Sweden, 1988.

[12] J. Delsing, "Method and apparatus for measuring mass flow," U.S. Patent 5 214 966, 1993.

[13] J. van Deventer and J. Delsing, "An ultrasonic density probe," in *Proc. IEEE Ultrason. Symp.*, 1997, pp. 871–875.

[14] E. Bjørndal and K.-E. Frøysa, "Acoustic methods for obtaining the pressure reflection coefficient from a buffer rod based measurement cell," *IEEE Trans. Ultrason., Ferroelect., Freq. Contr.*, vol. 55, no. 8, pp. 1781–1793, Aug. 2008.

[15] W. Kester, "Which ADC architecture is right for your application?," Analog Dialogue 39-06, June 2005, Analog Devices. [Online]. Available: http://www.analog.com/.

[16] Agilent Technologies, "Agilent 54621A/22A/24A/41A/42A oscilloscopes and Agilent 54621D/22D/41D/42D mixed-signal oscilloscopes," User's Guide, pub. no. 54622-97036, 2002, pp. 4–19.

[17] W. Marczak, "Water as a standard in the measurement of speed of sound in liquids," *J. Acoust. Soc. Amer.*, vol. 102, no. 5, pp. 2776–2779, Nov. 1997.

[18] S. Leeman, L. Ferrari, J. P. Jones, and M. Fink, "Perspectives on attenuation estimation from pulse-echo signals," *IEEE Trans. Sonics Ultrason.*, vol. SU-31, no. 4, pp. 352–361, July 1984.

[19] K. Raum, A. Ozguler, S. A. Morris, and W. D. O'Brian, "Channel defect detection in food packages using integrated backscatter ultrasound imaging," *IEEE Trans. Ultrason., Ferroelect., Freq. Contr.*, vol. 45, no. 1, pp. 30–40, Jan. 1998.

[20] L. H. Le, "An investigation of pulse-timing techniques for broadband ultrasonic velocity determination in cancellous bone: A simulation study," *Phys. Med. Biol.*, vol. 43, pp. 2295–2308, 1998.

[21] A. O. Williams, "The piston source at high frequencies," *J. Acoust. Soc. Amer.*, vol. 23, no. 1, pp. 1–6, 1951.

[22] E. P. Papadakis, "Ultrasonic attenuation in thin specimens driven through buffer rods," *J. Acoust. Soc. Amer.*, vol. 44, no. 3, pp. 724–734, Apr. 1968.

[23] E. P. Papadakis, K. A. Fowler, and L. C. Lynnworth, "Ultrasonic attenuation by spectrum analysis of pulses in buffer rods: Method and diffraction corrections," *J. Acoust. Soc. Amer.*, vol. 53, no. 5, pp. 1336–1343, 1973.

[24] J. Kushibiki and M. Arakawa, "Diffraction effects on bulk-wave ultrasonic velocity and attenuation measurements," *J. Acoust. Soc. Amer.*, vol. 108, no. 2, pp. 564–573, Aug. 2000.

[25] N. Hoppe, A. Püttmer, and P. Hauptmann, "Optimization of buffer rod geometry for ultrasonic sensors with reference path," *IEEE Trans. Ultrason., Ferroelect., Freq. Contr.*, vol. 50, no. 2, pp. 170–178, Feb. 2003.

[26] J. P. Weight, "A model for the propagation of short pulses of ultrasound in a solid," *J. Acoust. Soc. Amer.*, vol. 81, no. 4, pp. 815–826, Apr. 1987.

[27] T. Lauwagie, H. Sol, G. Roebben, W. Heylen, Y. Shi, and O. Van der Biest, "Mixed numerical-experimental identification of elastic properties of orthotropic metal plates," *NDT Int.*, vol. 36, pp. 487–495, 2003.

[28] Z. Wang and A. Nur, "Ultrasonic velocities in pure hydrocarbons and mixtures," *J. Acoust. Soc. Amer.*, vol. 89, no. 6, pp. 2725–2730, June 1991.

[29] A. R. Selfridge, "Approximate material properties in isotropic materials," *IEEE Trans. Sonics Ultrason.*, vol. SU-32, no. 3, pp. 381–394, May 1985.

[30] J. van Deventer and J. Delsing, "Thermostatic and dynamic performance of an ultrasonic density probe," *IEEE Trans. Ultrason., Ferroelect., Freq. Contr.*, vol. 48, no. 3, pp. 675–682, May 2001.

[31] S. Gaisford, "Hydrocarbon mass flow meter," U.S. Patent 5 259 239, 1993.

[32] Available: http://www.cannoninstrument.com/home.htm.

[33] S. V. Gupta, "Dilatation of water and water density tables," in *Practical Density Measurement and Hydrometry*. M. Afsar, Ed. London: IOP, 2002, ch. 4, p. 100.

[34] E. Bjørndal, "Acoustic measurement of liquid density with applications for mass measurement of oil," Ph.D. dissertation, Univ. Bergen, Norway, 2007.

**Erlend Bjørndal** (M'05) was born in Bergen, Norway, on December 31, 1966. He received his diploma in electrical engineering in 1989 and the M.S. degree in physics in 1994 from the University of Bergen, Norway. He received the Ph.D. degree in physics from the University of Bergen, Norway, in 2007.

He worked at Aanderaa Instruments, Bergen, Norway from 1995 to 1997, and at READ Well Services, Bergen, Norway, from 1997 to 2001, as a development engineer. From 2001 until May 2007, he worked as a scientist at Christian Michelsen Research AS, Bergen, Norway, in the field of acoustic and electromagnetic sensing principles. He is presently employed at 3-Phase Measurements AS, Bergen, working as a project engineer. His research interests include acoustic transducer design, signal processing, and fluid characterization by acoustic means. He holds one patent in the field of acoustic measurement of liquid density.

Dr. Bjørndal is a member of the Norwegian Society of Chartered Technical and Scientific Professionals (Tekna).

**Kjell-Eivind Frøysa** was born in Aalesund, Norway, on November 16, 1963. He received the M.S. and the Ph.D. degrees in applied mathematics (theoretical acoustics) in 1987 and 1991, respectively, from the University of Bergen, Norway.

He has worked at Christian Michelsen Research AS, Bergen, Norway since 1993, as a scientist and later also as a program manager in the field of process instrumentation. His research interests include ultrasonic flow metering, ultrasonic quality measurement of oil and gas, ultrasonic process measurements, and propagation of acoustic waves through multiphase media. He holds one patent in the field of acoustic measurement of liquid density and has published several refereed papers in linear and nonlinear acoustics.

Dr. Frøysa is a member of the Norwegian Society of Oil and Gas Measurement (NFOGM) and the Norwegian Society of Chartered Technical and Scientific Professionals (Tekna).

**Svein-Atle Engeseth** was born in Bergen, Norway, on November 8, 1956. He received his diploma in electrical engineering in 1980 from Bergen University College and his M.S. degree in electrical engineering in 1982 from the School of Mines and Technology, Rapid City, SD.

From 1983 to 1987 he worked for Control Data Corporation in Minneapolis, MN. From 1987 to 1994 he was a teacher at Bergen University College, in 1995 he worked for Aanderaa Instruments, Bergen, 1996 to 2000 at Bergen University College, in 2001 for Nordic VLSI, Bergen, and from 2002 on at Bergen University College.